Published in final edited form as:

Cell Rep. 2022 November 01; 41(5): 111575. doi:10.1016/j.celrep.2022.111575.

Cholinergic receptor-Wnt pathway controls immune activation by sensing intestinal dysfunction

Jie Ren[1,2], **Yu Sang**[1,2], **Alejandro Aballay**[1,3,*]

[1]Department of Molecular Microbiology and Immunology, Oregon Health & Science University, Portland, OR, USA

[2]These authors contributed equally

[3]Lead contact

SUMMARY

Alterations in the intestinal physiology caused by pathogen colonization result in immune activation. To provide insights into the mechanisms underlying the control of immune activation by changes in intestinal homeostasis, we conducted a forward genetic screen for suppressors of immune activation by intestinal distension in *Caenorhabditis elegans*. Our results indicate that *C. elegans* ACC-4, a member of a family of acetylcholine receptors, is required in immune activation by defects in the defecation motor program or by pathogen infection. ACC-4 acts postsynaptically in non-cholinergic RIM neurons to regulate several immune genes and a Wnt-mediated host immune response. These findings uncover a gut-brain-microbial axis that uses neural cholinergic signaling and the Wnt pathway to control immune activation in response to alterations in intestinal homeostasis.

Graphical Abstract

*Correspondence: aballay@ohsu.edu.

AUTHOR CONTRIBUTIONS

J.R. and A.A. conceived and designed the experiments. J.S. and Y.S. performed the experiments. J.S., Y.S., and A.A. analyzed the data and wrote the paper.

SUPPLEMENTAL INFORMATION

Supplemental information can be found online at https://doi.org/10.1016/j.celrep.2022.111575.

DECLARATION OF INTERESTS

The authors declare no competing interests.

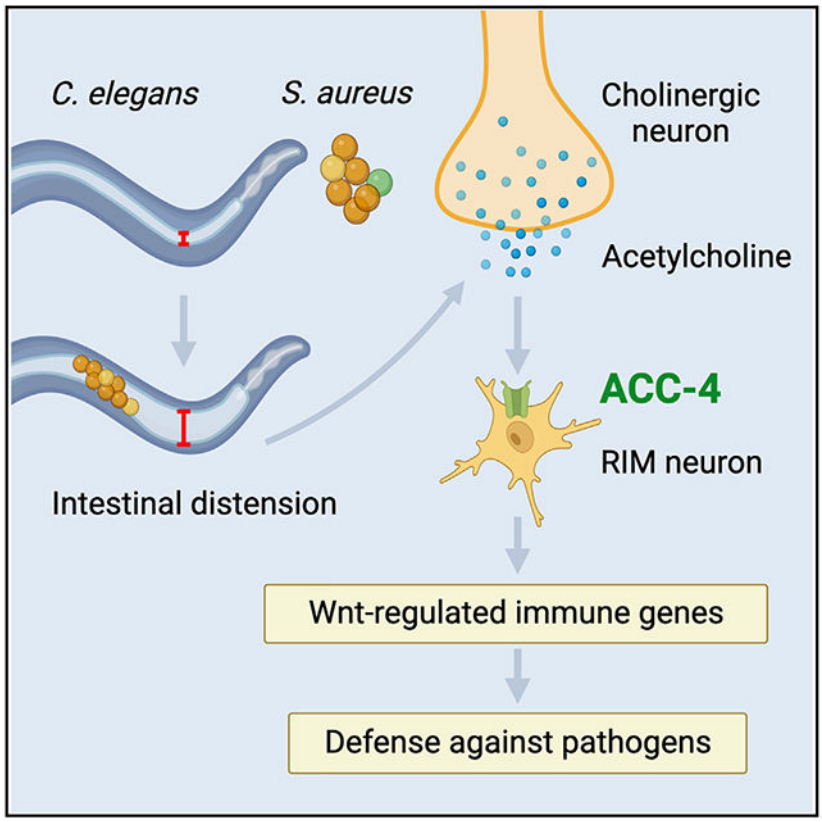

In brief

Ren et al. show that *C. elegans* ACC-4, a member of a family of acetylcholine receptors, is required in immune activation by intestinal distension or pathogen infection. ACC-4 functions in non-cholinergic RIM neurons to regulate immune genes, including Wnt-regulated genes.

INTRODUCTION

The ability to differentiate pathogenic from non-pathogenic microbes is an essential step in the elicitation of an appropriate immune response. Recent evidence indicates that intestinal distension caused by bacterial colonization activates a broad innate immune response (Singh and Aballay, 2019b). This innate immune activation depends on inputs from the intestine that can facilitate a wide range of interactions between the host and diverse microbes and provoke host responses using a neuralgut axis that maintains immune homeostasis.

Intestinal microbes may affect host behavior through metabolic compounds but also regulate levels of host neurotransmitters (Strandwitz, 2018). In particular, some members of the microbiota have the ability to sense, synthesize, or catabolize neurotransmitters (Strandwitz, 2018). Acetylcholine (ACh) is the predominant neurotransmitter in the enteric nervous system (Harrington et al., 2010). It is known to regulate various biological processes, including learning, memory consolidation, gut physiology, the integumentary system, and the cardiovascular system (Deng and Jiang, 2021; Hasselmo, 1999, 2006; Hirota and McKay, 2006). In addition to cholinergic neurons, various non-neuronal cell types can also

generate acetylcholine (Saracino et al., 2013; Wessler and Kirkpatrick, 2008), including immune cells, such as T cells expressing choline acetyltransferase that can directly release acetylcholine (Cox et al., 2019; Rosas-Ballina et al., 2011).

Mammals express two types of ACh receptors: muscarinic acetylcholine receptors, which are G-protein-coupled receptors (GPCRs), and nicotinic acetylcholine receptors, which are ligand-gated ion channels belonging to the cys-loop family (Treinin and Jin, 2021). *Caenorhabditis elegans* has many ACh receptors, including at least four ACh-gated chloride channels that are part of the cys-loop receptor family (Dittman and Kaplan, 2008; Putrenko et al., 2005). Receptors of the cys-loop family constitute a major class of receptor-coupled ion channels. They contain five protein subunits, each harboring a signature sequence of 13 residues flanked by cysteines, which bond covalently to form a closed loop situated between binding and channel domains (Sine and Engel, 2006). Each receptor has three domains: an extracellular domain that contains the ligand-binding sites, a transmembrane domain that allows ions to pass across the membrane, and an intracellular domain that plays a role in channel conductance and receptor modulation (Bondarenko et al., 2022). Cys-loop receptors are the major targets for many active compounds, including anesthetics, muscle relaxants, and a range of drugs that treat neurological disorders such as Alzheimer's disease (Thompson et al., 2010).

We conducted a forward genetic screen to uncover neuronal regulatory mechanisms involved in controlling immune activation by intestinal distension in *C. elegans*. We found that mutants in *acc-4*, which encodes a predicted ACh-gated chloride (ACC) channel, are deficient in immune activation. As a consequence, human bacterial pathogens *Staphylococcus aureus* and *Pseudomonas aeruginosa* caused more severe infections in *acc-4* mutants than in wild-type animals. ACC-4 was required in non-cholinergic RIM neurons to regulate the Wnt-mediated host immune response. Our findings uncovered a function for the cholinergic receptor ACC-4 in RIM neurons during immune activation, indicating that neural cholinergic signaling plays a key role in the modulation of host immune defenses that promote survival during infections. These studies are critical to better understand the neural circuits responsible for integrating cues that alert the nervous system in response to changes in intestinal physiology.

RESULTS

Acetylcholine receptor ACC-4 is required for immune activation during intestinal distension

Because alterations in the intestinal physiology caused by pathogen accumulation and subsequent distension of the intestinal lumen of *C. elegans* are critical for the expression of immune genes (Singh and Aballay, 2019a, 2019b), we performed a forward genetic screen to identify genes involved in the control of immune activation by intestinal distension. We used RNAi to inhibit the gene *aex-5*, which encodes a furin-like prohormone convertase that is involved in the defecation motor program (DMP). Downmodulation of *aex-5* causes intestinal distension and subsequent activation of immune genes, including *clec-60*, which encodes a secreted C-type lectin (Singh and Aballay, 2019a). We used strain JIN810, which takes advantage of the clec-60 promoter to express green fluorescent protein (GFP) in the

C. elegans intestine. The screen of 30,000 F2 progeny of ethyl methanesulfonate (EMS) mutagenized JIN810 animals yielded 13 mutants exhibiting reduced GFP signal (Figure 1A). Eight mutants showing strong defects in immune activation (weak GFP signal) after being backcrossed four times (Figure 1B) were sequenced.

After comparing mutant genome DNA sequences to the parental strain JIN810, linkage maps of single-nucleotide polymorphisms (SNPs) were obtained (Figure S1). Analysis of the protein-coding genes carrying mutations in the mapped region of mutant number 110 (AY164) revealed a single G→A mutation (G160A) in the *acc-4* gene in the *C. elegans* genome leading to an alanine (A) to threonine (T) substitution at residue 54. ACC-4 is an acetylcholine-gated chloride channel subunit that may form heteromers with other ACh-gated chloride channel subunits (Putrenko et al., 2005).

To confirm that the decreased GFP signal in the mutant was caused by reduced activity of the *clec-60* promoter rather than a mutation in the *gfp* sequence, we tested the endogenous expression of *clec-60* in the *acc-4(ac110)* background. As shown in Figure 1C, the *clec-60* expression increased by *aex-5* RNAi is lower in the *acc-4(ac110)* background than in the parental strain (Figure 1C). Even though *clec-60* expression during intestinal distension is highly impaired in the *acc-4(ac110)* background, the A to T substitution is neither in the acetylcholine binding domain nor in the ion channel. However, alanine is an amino acid with hydrophobic side chains, while threonine is an amino acid with polar uncharged side chains, and A to T substitutions affect overall protein folding (van Dijk et al., 2015) and quaternary organization (Podoly et al., 2010).

To confirm that the decreased activation of *clec-60* was indeed due to mutation in the *acc-4* gene, we studied *acc-4(ok2371)* animals carrying a 1,982-base pair (bp) deletion ranging from −181 bp to 1,801 bp in the genomic DNA. *acc-4(ok2371)* animals showed a significant decrease in *clec-60* mRNA levels compared with wild-type animals (Figure 1D). These results indicated that ACC-4 was required for DMP dysfunction-induced *clec-60* activation.

We reasoned that animals carrying *acc-4* mutation would show decreased resistance to infection because of blocked immune activation. To test this hypothesis, we used gram-negative *P. aeruginosa* and gram-positive *S. aureus* human bacterial pathogens. As shown in Figures 1E and 1F, both *acc-4(ac110)* and *acc-4(ok2371)* mutants were more susceptible to infections by *S. aureus* and *P. aeruginosa* than wild-type animals.

To further confirm that lack of functional ACC-4 caused the deficiency in immune activation, we expressed ACC-4 in the *acc4(ac110)* background under the regulation of its own promoter. As shown in Figures 1G and 1H, expression of *acc-4* rescued the deficient GFP fluorescence of the *acc-4(ac110)* background to levels that were comparable to control animals. Next, we tested whether ACC-4 expression under the regulation of its own promoter could rescue the decreased endogenous *clec-60* mRNA level of *acc-4* animals in response to dysfunction in DMP. ACC-4 expression under the regulation of its own promoter rescued the reduced *clec-60* level of the *acc-4(ac110)* background (Figure 1I). We also created *acc4(ok2371)* animals expressing ACC-4 under the regulation of its own promoter. Neither DMP dysfunction caused by *aex-5* RNAi nor *S. aureus* infection

changed the pattern of ACC-4 expression (Figures S2A and S2B). As shown in Figure 1J, the decreased endogenous *clec-60* mRNA levels of *acc-4(ok2371)* animals were completely rescued by the expression of ACC-4. These results indicated that ACC-4 was required for DMP dysfunction-induced *clec-60* activation.

Cholinergic activation of *clec-60* is mediated by ACC-4

To determine whether activation of *clec-60* was ACh dependent, we used the ACh-mimic compound arecoline (Gilani et al., 2004). Administration of arecoline to uninfected (*E. coli*-fed) animals was sufficient to induce *clec-60p*::*gfp* expression (Figures 2A and 2B), while the antagonist scopolamine (Hwang et al., 1999) impaired *clec-60p*::*gfp* induction by arecoline (Figures 2A and 2B). Arecoline activates *clec-60* without causing intestinal distension (Figure S3). Arecoline failed to activate GFP fluorescence in the *acc-4(ac110)* background (Figures 2C and 2D). Expression of ACC-4 under the regulation of its own promoter in the *acc-4(ac110)* background rescued the activation of GFP fluorescence by arecoline (Figures 2E and 2F), and the recovered GFP activation was inhibited by scopolamine (Figures 2E and 2F).

Consistent with the changes in GFP (Figures 2A-2F), the endogenous *clec-60* mRNA level was significantly induced after arecoline treatment and suppressed by the antagonist scopolamine in *clec-60p*::*gfp* animals (Figure 2G). In the *acc-4(ac110)* background, in contrast, the mRNA level of *clec-60* was not activated by arecoline (Figure 2G). ACC-4 expression under the regulation of its own promoter fully rescued the reduced *clec-60* level of the *acc-4(ac110)* background (Figure 2G). ACC-4 expression under the regulation of its own promoter also fully rescued the mutant phenotype of *acc-4(ok2371)* animals exposed to arecoline (Figure 2H). In addition, the induction of *clec-60* by arecoline was inhibited by the antagonist scopolamine (Figures 2G and 2H). These results showed that ACC-4 was required for ACh-dependent activation of *clec-60*, suggesting that the cholinergic nervous system was involved in activating *clec-60*, and that ACC-4 mediated immune activation by acetylcholine release.

ACC-4 is required for *S. aureus* infection-induced *clec-60* expression and resistance against infection

A strong immune response is activated in *C. elegans* intestinal epithelial cells after *S. aureus* infection (Irazoqui et al., 2010). As shown in Figures 3A-3D, the *acc-4(ac110)* background inhibited the *S. aureus*-activated GFP fluorescence, and the defect in *S. aureus*-activated GFP fluorescence was recovered when *acc-4* was expressed under the regulation of its own promoter (Figures 3E and 3F). The antagonist scopolamine impaired GFP fluorescence induced by *S. aureus* in the rescued strain (Figures 3E and 3F). The endogenous *clec-60* mRNA level was significantly induced after *S. aureus* infection and suppressed by the antagonist scopolamine in *clec-60p*::*gfp* animals, while the endogenous mRNA level of *clec-60* was not activated by *S. aureus* in the *acc-4(ac110)* background (Figure 3G). ACC-4 expression under the regulation of its own promoter fully rescued the reduced *clec-60* level of the *acc-4(ac110)* background (Figure 3G). ACC-4 expression under the regulation of its own promoter also fully rescued the deficient *clec-60* expression of *acc-4(ok2371)* animals

exposed to *S. aureus* (Figure 3H). In addition, activation of *clec-60* expression was inhibited by scopolamine (Figures 3G and 3H).

Consistent with the aforementioned changes in *clec-60* expression, ACC-4 expression driven by its own promoter rescued the enhanced susceptibility of *acc-4(ok2371)* animals to *S. aureus* (Figure S4). Collectively, these results showed that ACC-4 was required for *clec-60* activation by exposure to *S. aureus* and resistance against infection.

ACC-4 functions in RIM neurons to control immune activation

ACC-4 is expressed in the nervous system (Blazie et al., 2017; Pereira et al., 2015; Taylor et al., 2021; Von Stetina et al., 2007; Wang et al., 2015) from where it is likely to control immune activation. To test this hypothesis, we created strain AY163 to enhance neuronal *acc-4* RNAi by introducing *unc-119p*::*sid-1* into JIN810 (*clec-60p*::*gfp*) animals. The neural recalcitrancy to RNAi can be circumvented by expressing SID-1 in the nervous system to enable passive double-strand RNA neuronal uptake (Shih and Hunter, 2011). Strain AY163 exhibited a significant decrease in GFP fluorescence by *acc-4* RNAi in the model of intestinal lumen distension induced by defects in the DMP (Figures 4A and 4B), while no decrease in fluorescence by *acc-4* RNAi was observed in control JIN810 (*clec-60p*::*gfp*) animals (Figures 4C and 4D). *unc-22* RNAi was used as a negative control to indicate that RNAi on a second gene did not affect the impact of *aex-5* RNAi in eliciting DMP dysfunction-induced *clec-60* activation. Also, *acc-4* expression was significantly inhibited by RNAi in both JIN810 (*clec-60p*::*gfp*) and AY163 (*clec-60p*::*gfp*;*unc-119p*::*sid-1*) animals (Figure S5). These results suggested that ACC-4 functioned in neurons to activate *clec-60*.

The neurotransmitter ACh is synthesized in cholinergic neurons (Rand, 2007). ACC-4, as an ACh receptor (Putrenko et al., 2005), may function as a presynaptic or postsynaptic receptor to regulate intestinal distension-induced immune activation in response to acetylcholine release. Within 18 ACC-4-expressing neurons (Blazie et al., 2017; Pereira et al., 2015; Taylor et al., 2021; Von Stetina et al., 2007; Wang et al., 2015), four neurons, RIS, RIM, AVF, and I5, are non-cholinergic neurons, while the others are cholinergic neurons. As a first step to studying where ACC-4 functions to control immune activation in response to intestinal distension, we focused on candidate neurons from the smaller group of non-cholinergic neurons. We used Wormweb (http://wormweb.org/) to identify genes reported to be uniquely expressed in RIS, RIM, AVF, or I5 and found that RIM was the only neuron to have reported a uniquely expressed gene, *gcy-13*. Because *gcy-13* is a member of a family of genes encoding guanylyl cyclases that are essential for neural function (Hallem et al., 2011; Huang et al., 2020; Li and van der Kooy, 2018; Maruyama, 2016; Zimmer et al., 2009), we analyzed the *clec-60* mRNA levels in DMP-deficient animals carrying a mutation in *gcy-13*. We found that *clec-60* could not be activated in *gcy-13(gk3189)* animals deficient in DMP (Figure 4E). Thus, we reasoned that ACC-4 might function in RIM neurons and studied a second gene, *tdc-1*, that encodes a tyrosine decarboxylase that is important for RIM function (Alkema et al., 2005). In *tdc-1*(*n3420*) animals, we found that the expression of *clec-60* could not be activated by DMP dysfunction (Figure 4E). Moreover, both *gcy-13(gk3189)* and *tdc-1*(*n3420*) animals showed deficiencies in *clec-60* activation under arecoline treatment (Figure 4F) or *S. aureus* infection (Figure 4G). Therefore, we

reasoned that ACC-4 might function in RIM neurons to control intestinal distension-induced immune activation.

To study whether ACC-4 functions in RIM, we used 2.3 kb of the *gcy-13* promoter to express *acc-4* in RIM neurons in *acc-4(ok2371)* animals (Figure 5A). Even though it has been reported that *gcy-13* is only expressed in RIM (Ortiz et al., 2006), we found the *gcy-13* promoter drove the expression of *acc-4*::*gfp* to RIM and additional neurons (Figure 5A). However, those additional neurons do not express *acc-4* (Figures S6A and S6B). As shown in Figures 5B and 5C, ACC-4 expression under the regulation of *gcy-13* promoter rescued the reduced GFP fluorescence of the *acc-4(ac110)* background in the presence of *aex-5* RNAi. ACC-4 expression under the regulation of the *gcy-13* promoter could also partially rescue the decreased endogenous *clec-60* mRNA level of the *acc-4(ac110)* background in the presence of *aex-5* RNAi (Figure 5D). We also created *acc4(ok2371)* animals expressing ACC-4 under the regulation of the *gcy-13* promoter. As shown in Figure 5E, the decreased *clec-60* mRNA level in *acc-4(ok2371)* animals was rescued in these animals. We speculated that the expression of ACC-4 in RIM neurons could rescue immune activation not only by DMP dysfunction but also by exposure to arecoline or *S. aureus*. As shown in Figure S7 and Figure S8, ACC-4 expression under the regulation of the *gcy-13* promoter rescued the deficient GFP fluorescence of the *acc-4(ac110)* background treated with arecoline or infected by *S. aureus*. The decreased endogenous *clec-60* mRNA level of *acc-4(ok2371)* and *acc-4(ac110)* mutants exposed to arecoline or *S. aureus* was also rescued by expression of ACC-4 in RIM neurons (Figures S7 and S8). Consistent with the function of ACC-4 in RIM neurons to control immune activation, ACC-4 expression in RIM neurons rescued the enhanced susceptibility to *S. aureus* of the *acc-4(ac110)* background (Figures 5F and S4).

Canonical Wnt signaling is regulated by ACC-4 during *S. aureus* infection

Infection-induced ACh released from neurons stimulates muscarinic signaling in the epithelium, driving downstream induction of the canonical Wnt pathway and activation of *clec-60* (Labed et al., 2018). Therefore, we hypothesized that ACC-4 might control *clec-60* expression by regulating Wnt signaling. To test this hypothesis, we used reporter strain HS2332 (*cwn-2p*::*cwn-2*::*venus*) that expresses the *C. elegans* Wnt ligand encoding gene *cwn-2* fused to *venus*. We found that induction of *cwn-2*::Venus by *S. aureus* infection was inhibited by *acc-4* mutation (Figures 6A and 6B). We also studied the mRNA level of *cwn-2* and other Wnt signaling genes, *mig-1* and *bar-1*. These genes were induced during intestinal distension by *S. aureus* infection in an ACC-4-dependent manner (Figures 6C-6E). ACC-4 expression under the regulation of the *acc-4* or *gcy-13* promoter rescued the mutant phenotype of *acc-4(ok2371)* animals (Figures 6C-6E), indicating that Wnt signaling was involved in ACC-4-mediated immune activation during *S. aureus* infection.

We also studied whether ACC-4 was required for Wnt signaling induction by intestinal distension alone. We found that the induction of *cwn-2*::Venus by *aex-5* RNAi was inhibited by *acc-4* mutation (Figures S9A and S9B). In addition, the mRNA levels of *cwn-2*, *mig-1*, and *bar-1* induced by *aex-5* RNAi were also inhibited by *acc-4* mutation (Figures S9C-S9E). ACC-4 expression under the regulation of the *acc-4* or *gcy-13* promoters rescued the mutant

phenotype of *acc-4(ok2371)* animals (Figures S9C-S9E), indicating that Wnt signaling was involved in ACC-4-mediated immune activation during intestinal distension.

A previous work showed that GPCRs GAR-2/3 are required in the intestine for Wnt-mediated immune activation following *S. aureus* infection (Labed et al., 2018). Thus, we studied whether ACC-4 is part of the GAR-2/3 pathway that controls Wnt-mediated immunity. Activation by *S. aureus* infection of two out of three Wnt signaling genes (*cwn-2* and *bar-1*) was further inhibited in *acc-4(ok2371);gar-2/3* RNAi animals than in *acc-4(ok2371)* animals (Figures 6F-6H). The inhibition of *clec-60* expression upon *S. aureus* infection was also greater in *acc-4(ok2371);gar-2/3* RNAi animals than in *acc-4(ok2371)* animals (Figure 6I), suggesting that ACC-4 functions in parallel to GAR-2/3.

ACC-4 regulates a broad innate immune response during intestinal distension

Distension of the intestine by defects in DMP triggers the activation of innate immune genes, such as *clec-60*, *cpr-2*, *F53A9.8*, *ugt-18*, and *lys-5* (Singh and Aballay, 2019b), which are induced by bacterial pathogens capable of colonizing the intestine of the animals (Irazoqui et al., 2010; Luhachack et al., 2012). We speculated that ACC-4 controlled a series of innate immune genes in response to intestinal distension caused by *S. aureus* infection. We examined the expression of the genes *dod-20*, *dcf-17*, *sodh-1*, *cpr-2*, *ctl-2*, *lys-7*, *ilys-2*, *F53A9.8*, *ugt-18*, and *lys-5*, which are controlled by the DAF-16 (*dod-20*, *dcf-17*, *sodh-1*, *cpr-2*, *ctl-2*, and *F53A9.8*), SKN-1 (*sodh-1*, *ctl-2*, *ugt-18*, and *ilys-2*), ELT-2 (*F53A9.8*), and PMK-1 (*lys-5*) pathways. These immune genes were induced during intestinal distension by *S. aureus* infection in an ACC-4-dependent manner (Figure 7). To address whether ACC-4 controls innate immune gene expression during intestinal distension alone, we tested the expression of immune genes in *aex-5* RNAi animals fed *E. coli.* As shown in Figure S10, the expression of immune genes was induced by intestinal distension in an ACC-4-dependent manner. Therefore, ACC-4 regulated a broad innate immune response during intestinal distension.

DISCUSSION

This study demonstrates a mechanism of neuro-immune regulation in *C. elegans*. We propose that the cholinergic receptor ACC-4 is involved in acetylcholine-dependent neuro-immune regulation (Figure 7K). We discovered that the ACC-4-mediated neuronal signal could regulate immune activation during DMP dysfunction or *S. aureus* infection, suggesting that the accumulation of gut microbes in the intestine rather than specific bacteria may promote acetylcholine release. It remains unclear whether non-pathogenic microorganisms capable of causing intestinal colonization and distension may activate cholinergic signaling and subsequent immune activation. Indeed, intestinal distension and subsequent immune activation caused by colonization by probiotics may be part of the mechanism that mediates protection against microbial infections. For example, *Enterococcus faecium* colonization of *C. elegans* activates the Wnt/BAR-1 pathway (Sang et al., 2022).

In *C. elegans*, the ability to distinguish pathogenic from non-pathogenic microbes seems to require the integration of multiple cues, including oxygen level, odors, mechanosensation, pain, and the presence of alarmins to evaluate the environment and activate appropriate

immune responses. In mammals, the intestinal microbiota can affect host behavior by regulating dietary metabolic compounds like short-chain fatty acids (SCFAs). The SCFA receptors are expressed in the enteric nervous system (De Vadder et al., 2014), suggesting a role for these receptors in the activation of the nervous system by microbiota-regulated metabolic compounds. In addition, gut microbes can also directly regulate levels of host neurotransmitters (Strandwitz, 2018). Also, acetylcholine in the intestine is produced by both neurons and immune cells. The enzyme choline acetyltransferase expressed in T cells was found in the mouse gut after *Citrobacter rodentium* infection, and the expression of choline acetyltransferase by these cells was important for bacterial control (Ramirez et al., 2019). Therefore, T cell-derived acetylcholine aids host defenses during enteric bacterial infection. Our data indicated that bloating induced by bacterial colonization induced the release of acetylcholine in *C. elegans*.

Our studies demonstrate that neural cholinergic signaling serves as a key mechanism by which the nervous system controls intestinal host defense. Cholinergic signaling is critical for a number of physiological processes, and dysfunctional cholinergic receptors have been linked to a number of human conditions, including delirium, schizophrenia spectrum disorders, bipolar disorder, and Parkinson's, Huntington's, and Alzheimer's diseases (Caton et al., 2020; Foucault-Fruchard et al., 2018; Shimohama and Kawamata, 2018; Thomsen et al., 2011). Furthermore, cholinergic receptors are acknowledged as a potentially important therapeutic target for cardiovascular, psychiatric, and cognitive disorders (Dineley et al., 2015). Our results showed that the cholinergic receptor ACC-4 mediates the bacterial and intestinal distension-induced immune activation in *C. elegans* and suggest that cholinergic signaling could be a therapeutic target for treating intestinal infection and intestinal inflammatory conditions.

We found that the canonical Wnt pathway is regulated by the cholinergic receptor ACC-4 in *C. elegans*. The cholinergic-Wnt signaling axis appears to be evolutionarily conserved, as an endogenous cholinergic receptor has been shown to play a crucial role in a mouse Parkinson's disease model via regulation of Wnt/β-catenin signaling (Liu et al., 2017). Wnt signaling is responsible for inhibiting infections by pathogenic *Pseudomonas*, *Salmonella*, *Ehrlichia*, and *Mycobacterium* species (Blumenthal et al., 2006; Chen et al., 2016; Liu et al., 2011; Luo et al., 2015). Here, we found that the Wnt pathway was activated by intestinal distension, which was not limited to specific bacteria, highlighting that the conserved cholinergic receptor-Wnt pathway axis triggered the innate immune response to combat bacterial infection. Thus, cholinergic induction of the canonical Wnt pathway during pathogen infection is part of the so-called gut-brain-microbial axis, which is critical for maintaining host immune homeostasis.

Limitations of the study

To determine the specific foci of ACC-4 activity involved in the control of innate immunity, we studied the expression of immune-related genes and the pathogen susceptibility of *acc-4(ok2371)* animals expressing *acc-4* under the control of the *gcy-13* promoter. This promoter drives the expression of *acc-4* to RIM and additional neurons. Even though those other neurons do not express *acc-4*, the ectopic expression of *acc-4* might affect overall

neural signaling, leading to changes in gene expression and pathogen susceptibility. Also, given the large number of cholinergic neurons in the *C. elegans* nervous system, the identity of the cholinergic neuron/s acting upstream of RIM remains to be elucidated.

STAR★METHODS

RESOURCE AVAILABILITY

Lead contact—Further information and requests for resources and reagents should be directed to and will be fulfilled by the lead contact, Alejandro Aballay (aballay@ohsu.edu).

Materials availability—All reagents generated in this study are available from the lead contact upon request and without restriction.

Data and code availability

- The data reported in this paper will be shared by the lead contact upon request.
- This paper does not report original code.
- Any additional information required to reanalyze the data reported in this paper is available from the lead contact upon request.

EXPERIMENTAL MODEL AND SUBJECT DETAILS

The *C. elegans* strains were cultured under standard conditions and fed *E. coli* OP50. All *C. elegans* strains were maintained on nematode growth medium (NGM) and fed *E. coli* strain OP50. The *C. elegans* strains wild-type N2 Bristol, JIN810 *agIs26* [*clec-60p*::*gfp* + *myo-2p*::*mCherry*], Tu3401 *uIs69* [*pCFJ90* (*myo-2p*::*mCherry*) + *unc-119p*::*sid-1*], CX12724[*acc-4(ok2371)*], and MT10661[*tdc-1(n3420)*], VC3242[*gcy-13(gk3189)*] were obtained from the *Caenorhabditis* Genetics Center (University of Minnesota, Minneapolis, MN). The following lines were constructed using standard genetic manipulation techniques: AY163 [*uls69;agls26*], AY164 [*acc-4(ac110)*);*agls26*], AY165 [*acc-4(ac110)*;*agls26;acc-4p*::*gfp*], AY166 [*acc-4(ac110)*;*agls26;gcy-13p*::*gfp*], AY167 [*acc-4(ok2371)*;*acc-4p*::*gfp*], AY168 [*acc-4(ok2371)*;*gcy-13p*::*gfp*]. Detailed strain information is listed in Table S1.

The following bacterial strains were used: *Escherichia coli* OP50, *E. coli* HT115(DE3), *Pseudomonas aeruginosa* PA14, and *Staphylococcus aureus* NCTCB325. Gram-negative bacteria were grown in Luria-Bertani (LB) broth. *Staphylococcus aureus* strain NCTCB325 was grown in tryptic soy broth prepared with nalidixic acid (10 μg/mL). All bacteria were grown at 37°C.

METHOD DETAILS

Forward genetic screen for mutants exhibiting reduced *clec-60* activation by *aex-5* RNAi—Ethyl methanesulfonate (EMS) mutagenesis was performed using the JIN810 strain, which expresses green fluorescent protein (GFP) in the posterior gut, and the GFP level increased on *aex-5* RNAi. Approximately 300 synchronized late L4 larvae of JIN810 were treated with 50 mM EMS for 4 h followed by washing with M9 buffer four times

for 1 h. The washed animals (P0 generation) were then transferred to large Petri dishes (10 cm) containing *E. coli* OP50, and these animals were allowed to lay eggs (F1 progeny) overnight. The animals corresponding to the P0 generation were then washed away with M9 buffer, and the F1 eggs that remained attached to the plates were self-fertilized and allowed to grow until adulthood. A total of 1,500 F1 gravid 1-day-old adults were transferred to *aex-5* RNAi-expressing bacterial lawns and allowed to lay eggs. After 2 h, the F1 gravid adults were removed, leaving 30,000 F2 eggs on 50 large Petri dishes. The F2s were allowed to develop into young adults on *aex-5* RNAi-expressing plates at 20°C. The animals that showed decreased GFP expression in the F2 progeny were selected on individual plates. All mutants were backcrossed four times with the parental JIN810 strain before analysis.

Fluorescence imaging—Animals were anesthetized using an M9 salt solution containing 40 mM sodium azide and mounted onto 2% agar pads. The animals were then visualized using a Leica M165 FC fluorescence stereomicroscope. Fluorescence images were captured using 50 msec, 100 msec, or 400 msec as indicated in figure legends. The GFP signal of eight animals per condition was quantified using Image J. The fluorescence of an entire animal was calculated using the following equation: corrected whole animal fluorescence = integrated density – (area of selected animal × mean fluorescence of background readings).

RNA interference—RNA interference (RNAi) was used to generate loss-of-function RNAi phenotypes by feeding the nematodes with *E. coli* strain HT115(DE3) expressing double-stranded RNA (dsRNA) homologous to a target gene (Fraser et al., 2000; Timmons and Fire, 1998). *E. coli* with the appropriate vectors were grown in LB broth containing ampicillin (100 mg/mL) and tetracycline (12.5 mg/mL) at 37°C overnight and plated onto NGM plates containing 100 mg/mL ampicillin and 3 mM isopropyl b-D-thiogalactoside (IPTG) (RNAi plates). RNAi-expressing bacteria were allowed to grow overnight at 37°C. Gravid adults were transferred to RNAi-expressing bacterial lawns and allowed to lay eggs for 2 h. The gravid adults were removed, and the eggs were allowed to develop at 20°C to young adults for subsequent assays. *unc-22* RNAi was included as a positive control to account for the RNAi efficiency. All RNAi clones were from the Ahringer RNAi library.

Whole-genome sequencing and data analysis for the identification of *acc-4*—For whole-genome sequencing, the DNA of the mutant animals was extracted. Briefly, the mutants were grown at 20°C on 10 cm NGM plates seeded with *E. coli* OP50. These animals were grown until starvation, and then the plates were rinsed three times with M9 buffer to remove any bacteria. Then, the animals were incubated in M9 buffer with rotation for 2 h and washed three times with M9 buffer to remove bacteria from the intestine. The genomic DNA was extracted using the Gentra Puregene kit (QIAGEN, Netherlands). The DNA was subjected to whole-genome sequencing (WGS) on an Illumina HiSeq 4000 sequencing platform using 50 single-end nucleotide reads, and DNA libraries were prepared according to a standard Illumina (San Diego, CA) protocol. Library preparation and WGS were performed at Novogene Genomic Services & Solutions Company, USA.

To analyze the whole-genome sequence data, the EMS density mapping workflow from the Cloud Map program of the Galaxy web platform was used (Minevich et al., 2012). A list of single nucleotide polymorphisms (SNPs) in the AY164 mutant was generated by

comparing mutant genome DNA with the parental strain JIN810 (Table S2). The common SNPs were removed, and linkage maps for the mutant were created (Figure S1). Analysis of SNPs for mutant AY164 showed linkage to chromosome III at 11Mb–14Mb (Figure S1). There were six genes in this region (*Y41C4A.11*, *tbx-38*, *spin-4*, *gab-1*, *lgc-37*, and *acc-4*) (Table S2). We focused on *acc-4* because it is the only gene found in the 13Mb–14Mb region corresponding to the gray bar that shows the highest frequency of SNPs (Figure S1 and Table S2). The role of *acc-4* in *clec-60p*::*GFP* activation during intestinal distension was confirmed using neural-enhanced RNAi and *acc-4(ok2371)* animals.

***Staphylococcus aureus* infection—**The bacterial lawns were prepared by inoculating individual bacterial colonies into 5 mL of tryptic soy broth with nalidixic acid (10 μg/mL) and growing them overnight on a shaker at 37°C. Then, the overnight *S. aureus* culture was diluted 1:10, and 20 μL of the diluted culture was plated onto a 3.5-cm plate and incubated at 37°C for 6 h. Plates were cooled to room temperature for at least 1 h before seeding with synchronized young adult animals. The killing assays were performed at 25°C, and live animals were transferred daily to fresh plates. Animals were scored at the times indicated and were considered dead when they failed to respond to touch. Each experiment was performed in triplicate (n = 90 animals). For GFP imaging or qRT-PCR, animals were harvested at 16 h postinfection.

***C. elegans* killing assays on *Pseudomonas aeruginosa* PA14—**The bacterial lawns used for *C. elegans* killing assays were prepared by spreading 20 μL of an overnight culture of.

P. aeruginosa PA14 grown at 37°C on the complete surface of modified NGM agar medium (0.35% peptone instead of 0.25% peptone) in 3.5-cm-diameter plates. The plates were incubated at 37°C for 12 to 16 h and then cooled to room temperature for at least 1 h before seeding with synchronized young adult animals. The killing assays were performed at 25°C, and live animals were transferred daily to fresh plates. Animals were scored at the times indicated and were considered dead when they failed to respond to touch. Each experiment was performed in triplicate (n = 90 animals).

Drug treatments—Arecoline hydrobromide (Sigma, 31593–250MG) was dissolved in PBS to make a 200 mM stock solution, which was subsequently diluted 1:40 (5 mM working concentration) and added to 55°C NGM agar medium before preparing individual plates. 100 μL of 10×concentrated overnight culture of OP50 was seeded on solidified arecoline-containing NGM plates and incubated at 25°C overnight. Scopolamine (Sigma PHR1470-500MG) was dissolved in ddH_2O (200 mM stock solution, 5mM working concentration) and added to 55°C NGM agar medium together with arecoline. For *S. aureus* infections under the presence of scopolamine, 5 mM scopolamine was added to 55°C tryptic soy agar medium. The animals did not exhibit any visible motility difference at the concentrations used. Animals were treated at the young adult stage and incubated at 25°C for 16 h. After 16 h, animals were harvested for imaging or qRT-PCR.

Cloning and generation of transgenic *C. elegans* strains—For *acc-4* rescue, recombinant plasmid pPD95.77_*acc-4p*::*acc-4*_SL2::*gfp* was constructed by cloning

gene *acc-4* with its 2,014-bp promoter into the *Pst*I and *BamH*I sites of the pPD95.77_SL2::*gfp* vector (Cao et al., 2017). For RIM-specific *acc-4* rescue, plasmid pPD95.77_*gcy-13p*::*acc-4*_SL2::*gfp* was constructed by inserting the fused 2.3-kb fragment of the *gcy-13* promoter sequence and 1,227-bp spliced *acc-4* encoding sequence into the *Sal*I and *BamH*I sites. Transgenic strains were created by injecting 25 ng/mL of the plasmids together with 50 ng/mL of the co-injection marker *unc-122p*::*rfp*.

RNA isolation and quantitative reverse transcription-PCR (qRT-PCR)—The animals fed on *aex-5* RNAi plates or treated with *S. aureus* or arecoline following the above-described protocol were collected, washed with M9 buffer, and frozen in QIAzol reagent (Qiagen, Netherlands). Total RNA was extracted using the RNeasy Plus Universal kit (Qiagen, Netherlands). A total of 6 μg of total RNA was reverse transcribed with random primers using the High-Capacity cDNA reverse transcription kit (Applied Biosystems, Foster City, CA).

Quantitative reverse transcription-PCR (qRT-PCR) was conducted using the Applied Biosystems one-step real-time PCR protocol using SYBR green fluorescence (Applied Biosystems) on an Applied Biosystems 7900HT real-time PCR machine in 96-well plate format. Twenty-five-microliter reaction mixtures were analyzed as outlined by the manufacturer (Applied Biosystems). The relative fold changes of the transcripts were calculated using the comparative cycle threshold (C_T) ($2^{-\Delta\Delta CT}$) method and normalized to pan-actin (*act-1*, *act-3*, and *act-4*). The cycle thresholds of the amplification were determined using StepOnePlus software (Applied Biosystems). All samples were run in triplicate. The primer sequences are listed in Table S3.

QUANTIFICATION AND STATISTICAL ANALYSIS

The two-tailed Student's t-test for independent samples was used to analyze the data. To compare the means of more than two groups, one-way ANOVA with a post-hoc analysis was performed. All experiments were repeated at least 3 times, and error bars represent the standard deviation, unless otherwise indicated. The data were judged to be statistically significant when $p < 0.05$. 'n' represents the number of animals in each experiment. 'ns' indicates no significant difference, and the asterisk '*' indicates a significant difference; *$p < 0.05$, **$p < 0.01$, ***$p < 0.001$.

Supplementary Material

Refer to Web version on PubMed Central for supplementary material.

ACKNOWLEDGMENTS

This work was supported by NIH grants GM070977 and AI156900 (to A.A.). Some strains used in this study were provided by the Caenorhabditis Genetics Center (CGC), which is funded by the NIH Office of Research Infrastructure Programs (P40 OD010440).

INCLUSION AND DIVERSITY

We support inclusive, diverse, and equitable conduct of research.

REFERENCES

Alkema MJ, Hunter-Ensor M, Ringstad N, and Horvitz HR (2005). Tyramine functions independently of octopamine in the *Caenorhabditis elegans* nervous system. Neuron 46, 247–260. 10.1016/j.neuron.2005.02.024. [PubMed: 15848803]

Blazie SM, Geissel HC, Wilky H, Joshi R, Newbern J, and Mangone M (2017). Alternative polyadenylation directs fissue-specific miRNA targeting in *Caenorhabditis elegans* Somatic Tissues. Genetics 206, 757–774. 10.1534/genetics.116.196774. [PubMed: 28348061]

Blumenthal A, Ehlers S, Lauber J, Buer J, Lange C, Goldmann T, Heine H, Brandt E, and Reiling N (2006). The Wingless homolog WNT5A and its receptor Frizzled-5 regulate inflammatory responses of human mononuclear cells induced by microbial stimulation. Blood 108, 965–973. 10.1182/blood-2005-12-5046. [PubMed: 16601243]

Bondarenko V, Wells MM, Chen Q, Tillman TS, Singewald K, Lawless MJ, Caporoso J, Brandon N, Coleman JA, Saxena S, et al. (2022). Structures of highly flexible intracellular domain of human alpha7 nicotinic acetylcholine receptor. Nat. Commun 13, 793. 10.1038/s41467-022-28400-x. [PubMed: 35145092]

Cao X, Kajino-Sakamoto R, Doss A, and Aballay A (2017). Distinct roles of sensory neurons in mediating pathogen avoidance and neuropeptide-dependent immune regulation. Cell Rep. 21, 1442–1451. 10.1016/j.celrep.2017.10.050. [PubMed: 29117551]

Caton M, Ochoa ELM, and Barrantes FJ (2020). The role of nicotinic cholinergic neurotransmission in delusional thinking. NPJ Schizophr. 6, 16. 10.1038/s41537-020-0105-9. [PubMed: 32532978]

Chen K, Fu Q, Li D, Wu Y, Sun S, and Zhang X (2016). Wnt3a suppresses *Pseudomonas aeruginosa*-induced inflammation and promotes bacterial killing in macrophages. Mol. Med. Rep. 13, 2439–2446. 10.3892/mmr.2016.4869. [PubMed: 26846714]

Cox MA, Duncan GS, Lin GHY, Steinberg BE, Yu LX, Brenner D, Buckler LN, Elia AJ, Wakeham AC, Nieman B, et al. (2019). Choline acetyltransferase-expressing T cells are required to control chronic viral infection. Science 363, 639–644. 10.1126/science.aau9072. [PubMed: 30733420]

De Vadder F, Kovatcheva-Datchary P, Goncalves D, Vinera J, Zitoun C, Duchampt A, Bäckhed F, and Mithieux G (2014). Microbiota-generated metabolites promote metabolic benefits via gut-brain neural circuits. Cell 156, 84–96. 10.1016/j.cell.2013.12.016. [PubMed: 24412651]

Deng J, and Jiang H (2021). Role of nicotinic acetylcholine receptors in cardiovascular physiology and pathophysiology: current trends and perspectives. Curr. Vasc. Pharmacol 19, 370–378. 10.2174/1386207323666200917104920. [PubMed: 32940182]

Dineley KT, Pandya AA, and Yakel JL (2015). Nicotinic ACh receptors as therapeutic targets in CNS disorders. Trends Pharmacol. Sci 36, 96–108. 10.1016/j.tips.2014.12.002. [PubMed: 25639674]

Dittman JS, and Kaplan JM (2008). Behavioral impact of neurotransmitter-activated G-protein-coupled receptors: muscarinic and GABAB receptors regulate *Caenorhabditis elegans* locomotion. J. Neurosci 28, 7104–7112. 10.1523/JNEUROSCI.0378-08.2008. [PubMed: 18614679]

Foucault-Fruchard L, Tronel C, Bodard S, Gulhan Z, Busson J, Chalon S, and Antier D (2018).Alpha-7 nicotinic acetylcholine receptor agonist treatment in a rat model of Huntington's disease and involvement of heme oxygenase-1. Neural Regen. Res 13, 737–741. 10.4103/1673-5374.230301. [PubMed: 29722329]

Fraser AG, Kamath RS, Zipperlen P, Martinez-Campos M, Sohrmann M, and Ahringer J (2000). Functional genomic analysis of *C. elegans* chromosome I by systematic RNA interference. Nature 408, 325–330. 10.1038/35042517. [PubMed: 11099033]

Gilani AH, Ghayur MN, Saify ZS, Ahmed SP, Choudhary MI, and Khalid A (2004). Presence of cholinomimetic and acetylcholinesterase inhibitory constituents in betel nut. Life Sci. 75, 2377–2389. 10.1016/j.lfs.2004.03.035. [PubMed: 15350815]

Hallem EA, Spencer WC, McWhirter RD, Zeller G, Henz SR, Rätsch G, Miller DM 3rd, Horvitz HR, Sternberg PW, and Ringstad N (2011). Receptor-type guanylate cyclase is required for carbon dioxide sensation by *Caenorhabditis elegans*. Proc. Natl. Acad. Sci. USA 108, 254–259. 10.1073/pnas.1017354108. [PubMed: 21173231]

Harrington AM, Hutson JM, and Southwell BR (2010). Cholinergic neurotransmission and muscarinic receptors in the enteric nervous system. Prog. Histochem. Cytochem 44, 173–202. 10.1016/j.proghi.2009.10.001. [PubMed: 20159236]

Hasselmo ME (1999). Neuromodulation: acetylcholine and memory consolidation. Trends Cogn. Sci 3, 351–359. 10.1016/s1364-6613(99)01365-0. [PubMed: 10461198]

Hasselmo ME (2006). The role of acetylcholine in learning and memory. Curr. Opin. Neurobiol 16, 710–715. 10.1016/j.conb.2006.09.002. [PubMed: 17011181]

Hirota CL, and McKay DM (2006). Cholinergic regulation of epithelial ion transport in the mammalian intestine. Br. J. Pharmacol 149, 463–479. 10.1038/sj.bjp.0706889. [PubMed: 16981004]

Huang TT, Matsuyama HJ, Tsukada Y, Singhvi A, Syu RT, Lu Y, Shaham S, Mori I, and Pan CL (2020). Age-dependent changes in response property and morphology of a thermosensory neuron and thermotaxis behavior in *Caenorhabditis elegans*. Aging Cell 19, e13146. 10.1111/acel.13146. [PubMed: 32307902]

Hwang JM, Chang DJ, Kim US, Lee YS, Park YS, Kaang BK, and Cho NJ (1999). Cloning and functional characterization of a *Caenorhabditis elegans* muscarinic acetylcholine receptor. Recept. Channels 6, 415–424. [PubMed: 10635059]

Irazoqui JE, Troemel ER, Feinbaum RL, Luhachack LG, Cezairliyan BO, and Ausubel FM (2010). Distinct pathogenesis and host responses during infection of *C. elegans* by *P. aeruginosa* and *S. aureus*. PLoS Pathog. 6, e1000982. 10.1371/journal.ppat.1000982. [PubMed: 20617181]

Labed SA, Wani KA, Jagadeesan S, Hakkim A, Najibi M, and Irazoqui JE (2018). Intestinal epithelial Wnt signaling mediates acetylcholine-triggered host defense against infection. Immunity 48, 963–978.e3. 10.1016/j.immuni.2018.04.017. [PubMed: 29768179]

Li N, and van der Kooy D (2018). Mutations in the guanylate cyclase gcy-28 neuronally dissociate naive attraction and memory retrieval. Eur. J. Neurosci 48, 3367–3378. 10.1111/ejn.14221. [PubMed: 30362188]

Liu X, Wu S, Xia Y, Li XE, Xia Y, Zhou ZD, and Sun J (2011). Wingless homolog Wnt11 suppresses bacterial invasion and inflammation in intestinal epithelial cells. Am. J. Physiol. Gastrointest. Liver Physiol 301, G992–G1003. 10.1152/ajpgi.00080.2011. [PubMed: 21903761]

Liu Y, Hao S, Yang B, Fan Y, Qin X, Chen Y, and Hu J (2017). Wnt/beta-catenin signaling plays an essential role in alpha7 nicotinic receptor-mediated neuroprotection of dopaminergic neurons in a mouse Parkinson's disease model. Biochem. Pharmacol 140, 115–123. 10.1016/j.bcp.2017.05.017. [PubMed: 28551099]

Luhachack LG, Visvikis O, Wollenberg AC, Lacy-Hulbert A, Stuart LM, and Irazoqui JE (2012). EGL-9 controls *C. elegans* host defense specificity through prolyl hydroxylation-dependent and -independent HIF-1 pathways. PLoS Pathog. 8, e1002798. 10.1371/journal.ppat.1002798. [PubMed: 22792069]

Luo T, Dunphy PS, Lina TT, and McBride JW (2015). *Ehrlichia chaffeensis* exploits canonical and noncanonical host Wnt signaling pathways to stimulate phagocytosis and promote intracellular survival. Infect. Immun 84, 686–700. 10.1128/IAI.01289-15. [PubMed: 26712203]

Maruyama IN (2016). Receptor guanylyl cyclases in sensory processing. Front. Endocrinol 7, 173. 10.3389/fendo.2016.00173.

Minevich G, Park DS, Blankenberg D, Poole RJ, and Hobert O (2012). CloudMap: a cloud-based pipeline for analysis of mutant genome sequences. Genetics 192, 1249–1269. 10.1534/genetics.112.144204. [PubMed: 23051646]

Ortiz CO, Etchberger JF, Posy SL, Frøkjaer-Jensen C, Lockery S, Honig B, and Hobert O (2006). Searching for neuronal left/right asymmetry: genomewide analysis of nematode receptor-type guanylyl cyclases. Genetics 173, 131–149. 10.1534/genetics.106.055749. [PubMed: 16547101]

Pereira L, Kratsios P, Serrano-Saiz E, Sheftel H, Mayo AE, Hall DH, White JG, LeBoeuf B, Garcia LR, Alon U, and Hobert O (2015). A cellular and regulatory map of the cholinergic nervous system of *C. elegans*. Elife 4, e12432. 10.7554/eLife.12432. [PubMed: 26705699]

Podoly E, Hanin G, and Soreq H (2010). Alanine-to-threonine substitutions and amyloid diseases: butyrylcholinesterase as a case study. Chem. Biol. Interact 187, 64–71. 10.1016/j.cbi.2010.01.003. [PubMed: 20060816]

Putrenko I, Zakikhani M, and Dent JA (2005). A family of acetylcholine-gated chloride channel subunits in *Caenorhabditis elegans*. J. Biol. Chem 280, 6392–6398. 10.1074/jbc.M412644200. [PubMed: 15579462]

Ramirez VT, Godinez DR, Brust-Mascher I, Nonnecke EB, Castillo PA, Gardner MB, Tu D, Sladek JA, Miller EN, Lebrilla CB, et al. (2019). T-cell derived acetylcholine aids host defenses during enteric bacterial infection with *Citrobacter rodentium*. PLoS Pathog. 15, e1007719. 10.1371/journal.ppat.1007719. [PubMed: 30973939]

Rand JB (2007). Acetylcholine. WormBook, 1–21. 10.1895/wormbook.1.131.1.

Rosas-Ballina M, Olofsson PS, Ochani M, Valdés-Ferrer SI, Levine YA, Reardon C, Tusche MW, Pavlov VA, Andersson U, Chavan S, et al. (2011). Acetylcholine-synthesizing T cells relay neural signals in a vagus nerve circuit. Science 334, 98–101. 10.1126/science.1209985. [PubMed: 21921156]

Sang Y, Ren J, and Aballay A (2022). The transcription factor HLH-26 controls probiotic-mediated protection against intestinal infection through up-regulation of the Wnt/BAR-1 pathway. PLoS Biol. 20, e3001581. 10.1371/journal.pbio.3001581. [PubMed: 35263319]

Saracino L, Zorzetto M, Inghilleri S, Pozzi E, and Stella GM (2013). Non-neuronal cholinergic system in airways and lung cancer susceptibility. Transl. Lung Cancer Res 2, 284–294. 10.3978/j.issn.2218-6751.2013.06.01. [PubMed: 25806244]

Shih JD, and Hunter CP (2011). SID-1 is a dsRNA-selective dsRNA-gated channel. RNA 17, 1057–1065. 10.1261/rna.2596511. [PubMed: 21474576]

Shimohama S, and Kawamata J (2018). Roles of nicotinic acetylcholine receptors in the pathology and treatment of Alzheimer's and Parkinson's diseases. In Nicotinic Acetylcholine Receptor Signaling in Neuroprotection, Akaike A, Shimohama S, and Misu Y, eds. (Springer), pp. 137–158. 10.1007/978-981-10-8488-1_8.

Sine SM, and Engel AG (2006). Recent advances in Cys-loop receptor structure and function. Nature 440, 448–455. 10.1038/nature04708. [PubMed: 16554804]

Singh J, and Aballay A (2019a). Intestinal infection regulates behavior and learning via neuroendocrine signaling. Elife 8, e50033. 10.7554/eLife.50033. [PubMed: 31674907]

Singh J, and Aballay A (2019b). Microbial colonization activates an immune fight-and-flight response via neuroendocrine signaling. Dev. Cell 49, 89–99.e4. 10.1016/j.devcel.2019.02.001. [PubMed: 30827896]

Strandwitz P (2018). Neurotransmitter modulation by the gut microbiota. Brain Res. 1693, 128–133. 10.1016/j.brainres.2018.03.015. [PubMed: 29903615]

Taylor SR, Santpere G, Weinreb A, Barrett A, Reilly MB, Xu C, Varol E, Oikonomou P, Glenwinkel L, McWhirter R, et al. (2021). Molecular topography of an entire nervous system. Cell 184, 4329–4347.e23. 10.1016/j.cell.2021.06.023. [PubMed: 34237253]

Thompson AJ, Lester HA, and Lummis SCR (2010). The structural basis of function in Cys-loop receptors. Q. Rev. Biophys 43, 449–499. 10.1017/S0033583510000168. [PubMed: 20849671]

Thomsen MS, Weyn A, and Mikkelsen JD (2011). Hippocampal alpha7 nicotinic acetylcholine receptor levels in patients with schizophrenia, bipolar disorder, or major depressive disorder. Bipolar Disord. 13, 701–707. 10.1111/j.1399-5618.2011.00961.x. [PubMed: 22085484]

Timmons L, and Fire A (1998). Specific interference by ingested dsRNA. Nature 395, 854. 10.1038/27579. [PubMed: 9804418]

Treinin M, and Jin Y (2021). Cholinergic transmission in *C. elegans*: functions, diversity, and maturation of ACh-activated ion channels. J. Neurochem 158, 1274–1291. 10.1111/jnc.15164. [PubMed: 32869293]

van Dijk E, Hoogeveen A, and Abeln S (2015). The hydrophobic temperature dependence of amino acids directly calculated from protein structures. PLoS Comput. Biol 11, e1004277. 10.1371/journal.pcbi.1004277. [PubMed: 26000449]

Von Stetina SE, Watson JD, Fox RM, Olszewski KL, Spencer WC, Roy PJ, and Miller DM 3rd. (2007). Cell-specific microarray profiling experiments reveal a comprehensive picture of gene expression in the *C. elegans* nervous system. Genome Biol. 8, R135. 10.1186/gb-2007-8-7-r135. [PubMed: 17612406]

Wang J, Kaletsky R, Silva M, Williams A, Haas LA, Androwski RJ, Landis JN, Patrick C, Rashid A, Santiago-Martinez D, et al. (2015). Cell-specific transcriptional profiling of ciliated sensory neurons reveals regulators of behavior and extracellular vesicle biogenesis. Curr. Biol 25, 3232–3238. 10.1016/j.cub.2015.10.057. [PubMed: 26687621]

Wessler I, and Kirkpatrick CJ (2008). Acetylcholine beyond neurons: the non-neuronal cholinergic system in humans. Br. J. Pharmacol 154, 1558–1571. 10.1038/bjp.2008.185. [PubMed: 18500366]

Zimmer M, Gray JM, Pokala N, Chang AJ, Karow DS, Marletta MA, Hudson ML, Morton DB, Chronis N, and Bargmann CI (2009). Neurons detect increases and decreases in oxygen levels using distinct guanylate cyclases. Neuron 61, 865–879. 10.1016/j.neuron.2009.02.013. [PubMed: 19323996]

Highlights

- Acetylcholine-gated chloride channel ACC-4 controls immune activation
- ACC-4 mediates immune activation during intestinal dysfunction
- ACC-4 controls Wnt-regulated immune response
- ACC-4 functions in non-cholinergic RIM neurons to regulate the immune response

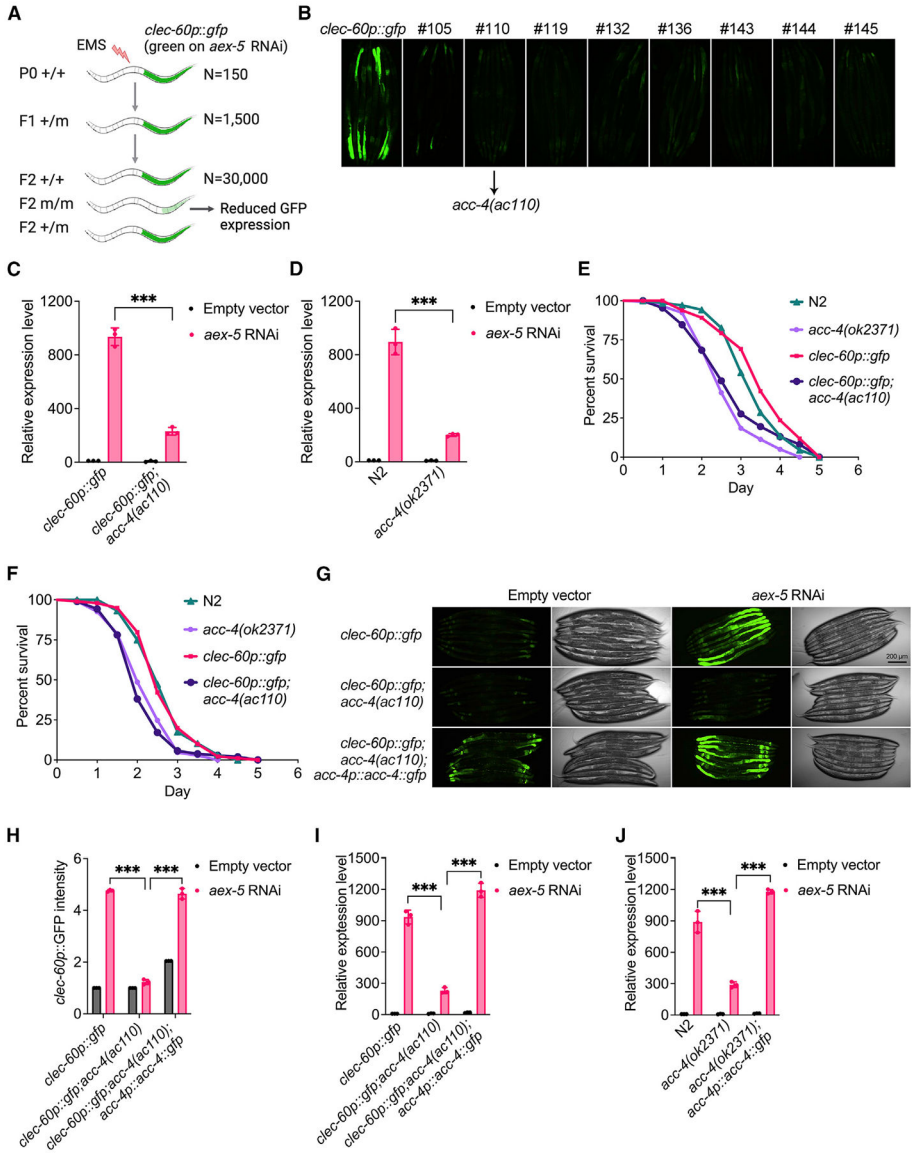

Figure 1. ACC-4 is required for immune activation induced by DMP dysfunction

(A) Schematic diagram of the forward genetic screen. Strain JIN810, carrying a transcriptional reporter for *clec-60* (*clec-60p*::*gfp*), was treated with ethyl methanesulfonate (EMS), and F1 animals were allowed to self-fertilize. F2 animals exhibiting decreased GFP signal in the presence of *aex-5* RNAi were picked.

(B) Photomicrographs of *clec-60p*::*gfp* animals and different *clec-60p*::*gfp* mutants exposed to *aex-5* RNAi (n = 8; representative of three independent experiments). Fluorescence images were captured using 50-ms exposure.

(C) Quantitative reverse transcription-PCR (qRT-PCR) analysis of the immune gene *clec-60* in *clec-60p*::*gfp* or *clec-60p*::*gfp*;*acc-4(ac110)* animals exposed to empty vector or *aex-5* RNAi. Data are the mean ± SEM from three independent experiments, n = 8 per condition. ***p < 0.001 via the t test.

(D) qRT-PCR analysis of the immune gene *clec-60* in wild-type N2 or *acc-4(ok2371)* animals exposed to empty vector or *aex-5* RNAi. Data are the mean ± SEM from three independent experiments, n ≈ 200 per condition. ***p < 0.001 via the t test.
(E) Survival of wild-type N2, *acc-4(ok2371)*, *clec-60p*::*gfp*, and *clec-60p*::*gfp*;*acc-4(ac110)* animals on *S. aureus* at 25°C. Data are the mean ± SEM from three independent experiments, n = 90 per condition. *clec-60p*::*gfp* versus *clec-60p*::*gfp*;*acc-4(ac110)*; p < 0.0001; N2 versus *acc-4(ok2371)*; p < 0.0001.
(F) Survival of wild-type N2, *acc-4(ok2371)*, *clec-60p*::*gfp*, and *clec-60p*::*gfp*;*acc-4(ac110)* animals on *P. aeruginosa* at 25°C. Data are the mean ± SEM from three independent experiments, n = 90 per condition. *clec-60p*::*gfp* versus *clec-60p*::*gfp*;*acc-4(ac110)*; p < 0.0001; N2 versus *acc-4(ok2371)*; p < 0.0001.
(G) Representative fluorescence micrographs of *clec-60p*::*gfp*, *clec-60p*::*gfp*;*acc-4(ac110)*, or *clec-60p*::*gfp*;*acc-4(ac110)*;*acc-4p*::*acc-4*::*gfp* exposed to vector control or *aex-5* RNAi (n = 8; representative of three independent experiments). Fluorescence images were captured using 50-ms exposure. Scale bar, 200 μm.
(H) Quantitative analysis of (G). The height of the column represents fold changes. Data are the mean ± SEM from three independent experiments, n = 8 per condition. ***p < 0.001 via the t test.
(I) qRT-PCR analysis of the immune gene *clec-60* in *clec-60p*::*gfp*, *clec-60p*::*gfp*;*acc-4(ac110)*, or *clec-60p*::*gfp*;*acc-4(ac110)*;*acc-4p*::*acc-4*::*gfp* animals exposed to vector control or *aex-5* RNAi. Data are the mean ± SEM from three independent experiments, n ≈ 200 per condition. ***p < 0.001 via the t test.
(J) qRT-PCR analysis of the immune gene *clec-60* in wild-type N2, *acc-4(ok2371)*, or *acc-4(ok2371)*;*acc-4p*::*acc-4*::*gfp* animals exposed to vector control or *aex-5* RNAi. Data are the mean ± SEM from three independent experiments, n ≈ 200 per condition. ***p < 0.001 via the t test.

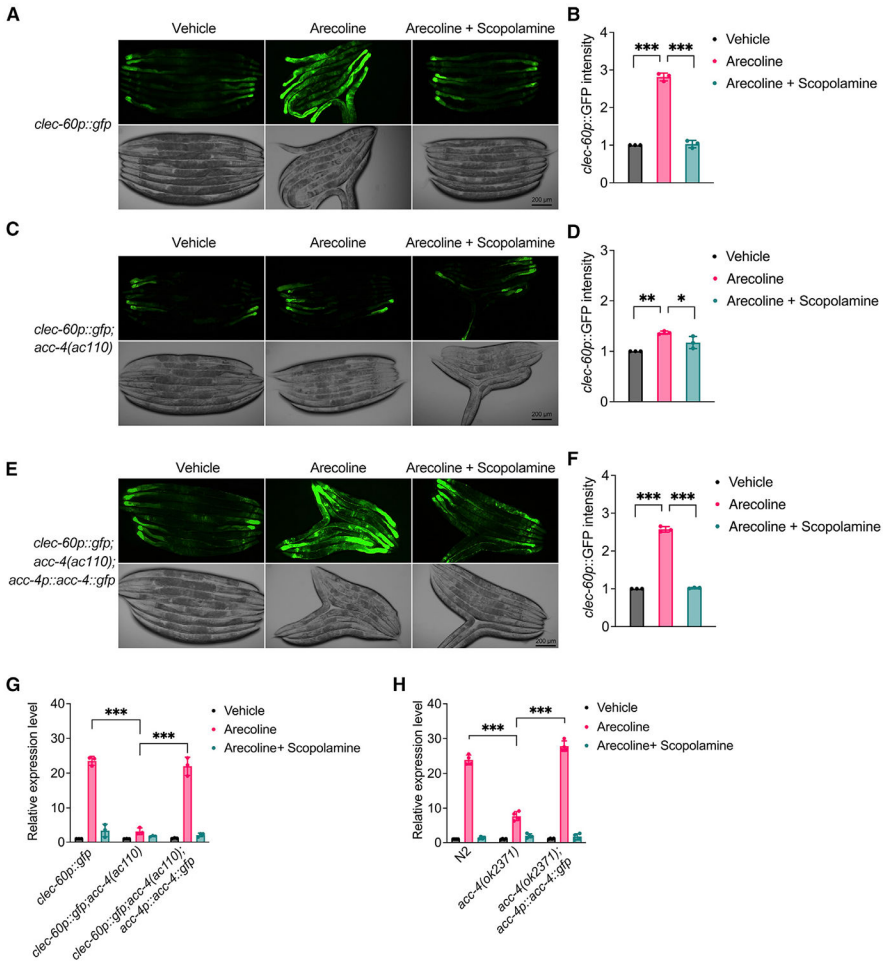

Figure 2. Expression of acc-4 rescues immune activation by arecoline treatment in *acc-4* mutants

(A) Representative fluorescence micrographs of *clec-60p*::*gfp* animals after 16 h of feeding on *E. coli* in the presence of vehicle (left), 5 mM arecoline (middle), or 5 mM arecoline plus 5 mM scopolamine (right). n = 8; representative of three independent experiments. Fluorescence images were captured using 50-ms exposure. Scale bar, 200 μm.

(B) Quantitative analysis of (A). The height of the columns represents fold change. Data are the mean ± SEM from three independent experiments, n = 8 per condition. ***p < 0.001 via the t test.

(C) Representative fluorescence micrographs of *clec-60p*::*gfp*;*acc-4(ac110)* animals after 16 h of feeding on *E. coli* in the presence of vehicle (left), 5 mM arecoline (middle), or 5 mM arecoline plus 5 mM scopolamine (right). n = 8; representative of three independent experiments. Fluorescence images were captured using 50-ms exposure. Scale bar, 200 μm.

(D) Quantitative analysis of (C). The height of the columns represents fold change. Data are the mean ± SEM from three independent experiments, n = 8 per condition. *p < 0.05 via the t test, **p < 0.01 via the t test.

(E) Representative fluorescence micrographs of *clec-60p*::*gfp*;*acc-4(ac110)*;*acc-4p*::*acc-4*::*gfp* animals after 16 h of feeding on *E. coli* in the presence of vehicle (left), 5 mM arecoline (middle), or 5 mM arecoline plus 5 mM

scopolamine (right). n = 8; representative of three independent experiments. Fluorescence images were captured using 50-ms exposure. Scale bar, 200 μm.

(F) Quantitative analysis of (E). The height of the columns represents fold change. Data are the mean ± SEM from three independent experiments, n = 8 per condition. ***p < 0.001 via the t test.

(G) qRT-PCR analysis of the immune gene *clec-60* in *clec-60p*::*gfp*, *clec-60p*::*gfp*;*acc-4(ac110)*, or *clec-60p*::*gfp*::*acc-4(ac110)*;*acc-4p*::*acc-4*::*gfp* animals after 16 h of feeding on *E. coli* in the presence of vehicle, 5 mM arecoline, or 5 mM arecoline plus 5 mM scopolamine. Data are the mean ± SEM from three independent experiments, n ≈ 200 per condition. ***p < 0.001 via the t test.

(H) qRT-PCR analysis of the immune gene *clec-60* in wild-type, *acc-4(ok2371)*, or *acc-4(ok2371)*;*acc-4p*::*acc-4*::*gfp* animals after 16 h of feeding on *E. coli* in the presence of vehicle, 5 mM arecoline, or 5 mM arecoline plus 5 mM scopolamine. Data are the mean ± SEM from three independent experiments, n ≈ 200 per condition. ***p < 0.001 via the t test.

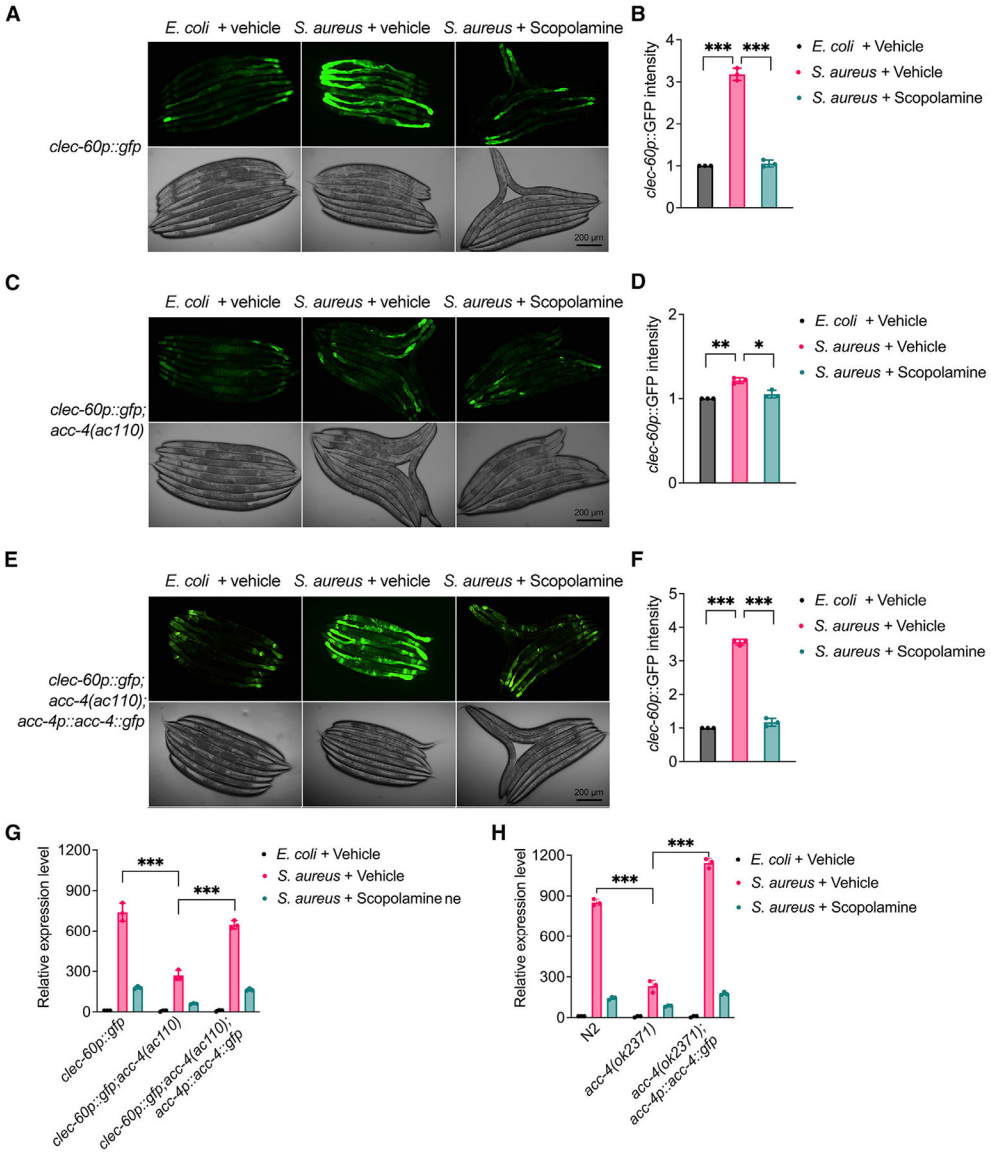

Figure 3. Expression of acc-4 rescues immune activation during *S. aureus* infection in *acc-4* mutants

(A) Representative fluorescence micrographs of *clec-60p*::*gfp* animals after 16 h in the presence of *E. coli* (left), *S. aureus* (middle), or 5 mM scopolamine with *S. aureus* (right). n = 8; representative of three independent experiments. Fluorescence images were captured using 50-ms exposure. Scale bar, 200 μm.

(B) Quantitative analysis of (A). The height of the column represents fold changes. Data are the mean ± SEM from three independent experiments, n = 8 per condition. ***p < 0.001 via the t test.

(C) Fluorescence micrographs of *clec-60p*::*gfp*;*acc-4(ac110)* animals after 16 h in the presence of *E. coli* (left), *S. aureus* (middle), or 5 mM scopolamine with *S. aureus* (right). n = 8; representative of three independent experiments. Fluorescence images were captured using 50-ms exposure. Scale bar, 200 μm.

(D) Quantitative analysis of (C). The height of the column represents fold changes. Data are the mean ± SEM from three independent experiments, n = 8 per condition. *p < 0.05, and **p < 0.01 via the t test.

(E) Fluorescence micrographs of *clec-60p*::*gfp*;*acc-4(ac110)*;*acc-4p*::*acc-4*::*gfp* animals after 16 h in the presence of *E. coli* (left), *S. aureus* (middle), or 5 mM scopolamine with *S. aureus* (right). n = 8; representative of three independent experiments. Fluorescence images were captured using 50-ms exposure. Scale bar, 200 μm.

(F) Quantitative analysis of (E). The height of the column represents fold changes. Data are the mean ± SEM from three independent experiments, n = 8 per condition. ***p < 0.001 via the t test.

(G) qRT-PCR analysis of the immune gene *clec-60* in *clec-60p*::*gfp*, *clec-60p*::*gfp*;*acc-4(ac110)*, or *clec-60p*::*gfp*;*acc-4(ac110)*;*acc-4p*::*acc-4*::*gfp* animals after 16 h in the presence of *E. coli*, *S. aureus*, or 5 mM scopolamine with *S. aureus*. Data are the mean ± SEM from three independent experiments, n ≈ 200 per condition. ***p < 0.001 via the t test.

(H) qRT-PCR analysis of the immune gene *clec-60* in wild-type, *acc-4(ok2371)*, or *acc-4(ok2371)*;*acc-4p*::*acc-4*::*gfp* animals after 16 h in the presence of *E. coli*, *S. aureus*, or 5 mM scopolamine with *S. aureus*. Data are the mean ± SEM from three independent experiments, n ≈ 200 per condition. ***p < 0.001 via the t test.

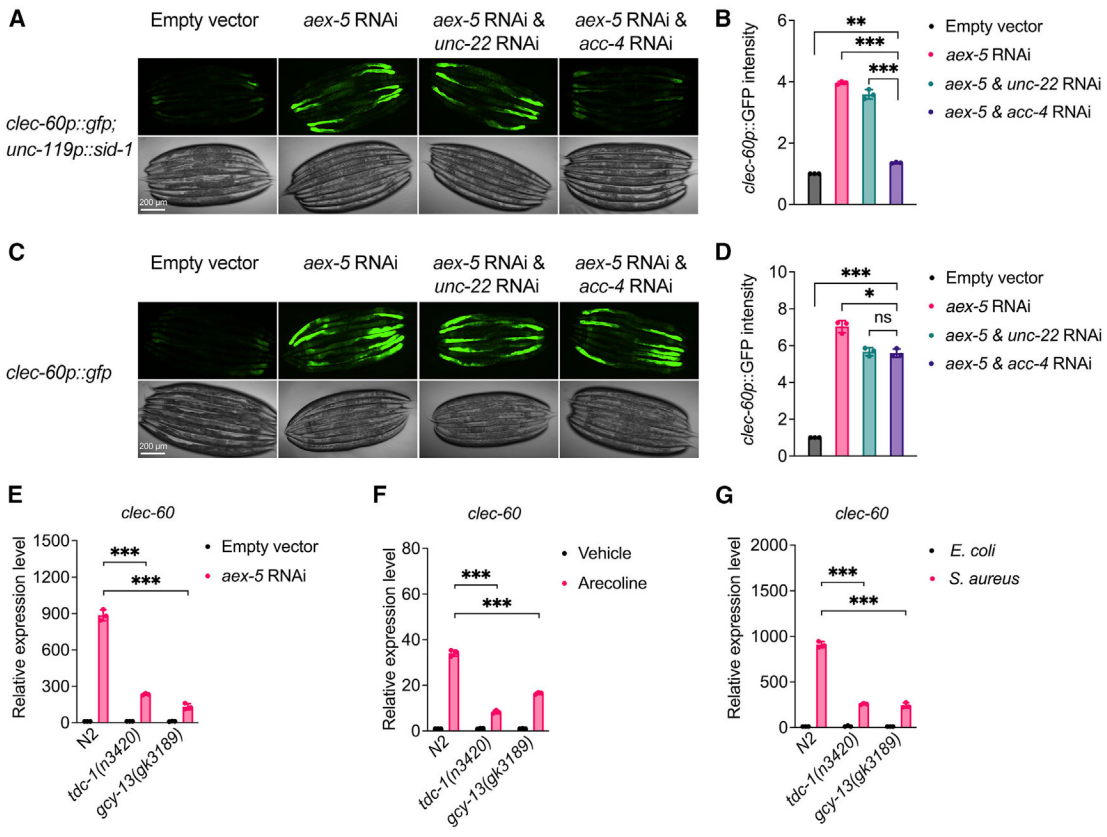

Figure 4. ACC-4 functions in neurons for immune activation

(A) Representative fluorescence micrographs of *clec-60p*::*gfp*;*unc-119p*::*sid-1* animals grown on bacteria carrying empty vector or RNAi against *aex-5*, *aex-5* and *unc-22*, or *aex-5* and *acc-4*. n = 8; representative of three independent experiments. Fluorescence images were captured using 50-ms exposure. Scale bar, 200 μm.

(B) Quantitative analysis of (A). The height of the columns represents fold changes. Data are the mean ± SEM from three independent experiments, n = 8 per condition. ***p < 0.001 via the t test.

(C) Representative fluorescence micrographs of *clec-60p*::*gfp* animals grown on bacteria carrying empty vector or RNAi against *aex-5*, *aex-5* and *unc-22*, or *aex-5* and *acc-4*. n = 8; representative of three independent experiments. Fluorescence images were captured using 50-ms exposure. Scale bar, 200 μm.

(D) Quantitative analysis of (C). The height of the columns represents fold changes. Data are the mean ± SEM from three independent experiments, n = 8 per condition. *p < 0.05, and **p < 0.01 via the t test. ns, non-significant.

(E) qRT-PCR analysis of the immune gene *clec-60* in wild-type N2, *tdc-1(n3420)*, or *gcy-13(gk3189)* animals grown on bacteria carrying empty vector or RNAi against *aex-5*. Data are the mean ± SEM from three independent experiments, n ≈ 200 per condition. ***p < 0.001 via the t test. ns, non-significant.

(F) qRT-PCR analysis of the immune gene *clec-60* in wild-type N2, *tdc-1(n3420)*, or *gcy-13(gk3189)* animals after 16 h feeding on *E. coli* in the presence of vehicle or 5 mM

arecoline. Data are the mean ± SEM from three independent experiments, n ≈ 200 per condition. ***p < 0.001 via the t test. ns, non-significant.

(G) qRT-PCR analysis of the immune gene *clec-60* in wild-type N2, *tdc-1(n3420)*, or *gcy-13(gk3189)* animals after 16 h of feeding on *E. coli* or *S. aureus*. Data are the mean ± SEM from three independent experiments, n ≈ 200 per condition. ***p < 0.001 via the t test. ns, non-significant.

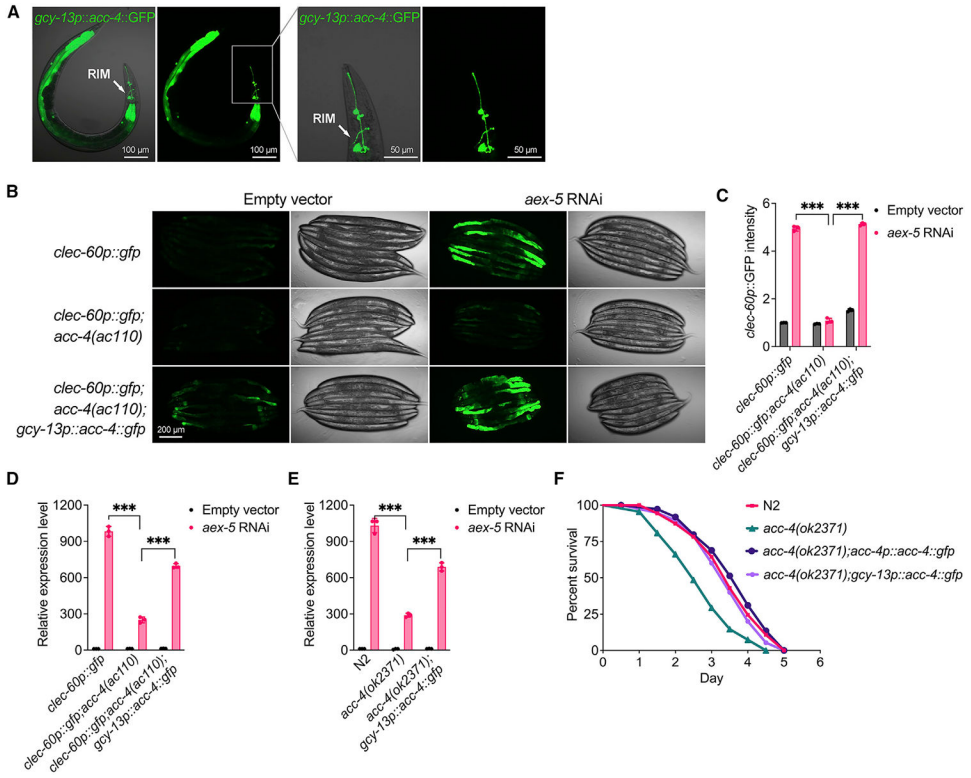

Figure 5. Expression of acc-4 in RIM rescues immune activation during DMP dysfunction

(A) Representative fluorescence micrographs of *acc-4(ok2371);gcy-13p*::*acc-4*::*gfp* animals. n = 30; representative of four independent experiments. Fluorescence images were captured using 400-ms exposure. Scale bars indicate 100 μm in the left two panels and 50 μm in the right two panels.

(B) Representative fluorescence micrographs of *clec-60p*::*gfp*, *clec-60p*::*gfp;acc-4(ac110)*, or *clec-60p*::*gfp;acc-4(ac110);gcy-13p*::*acc-4*::*gfp* animals grown on empty vector or *aex-5* RNAi. n = 8; representative of three independent experiments. Fluorescence images were captured using 50-ms exposure. Scale bar, 200 μm.

(C) Quantitative analysis of (B). The height of the columns represents fold changes. Data are the mean ± SEM from three independent experiments, n = 8 per condition. ***p < 0.001 via the t test.

(D) qRT-PCR analysis of the immune gene *clec-60* in *clec-60p*::*gfp*, *clec-60p*::*gfp;acc-4(ac110)*, or *clec-60p*::*gfp;acc-4(ac110);gcy-13p*::*acc-4*::*gfp* animals grown on empty vector or *aex-5* RNAi. Data are the mean ± SEM from three independent experiments, n ≈ 200 per condition. ***p < 0.001 via the t test.

(E) qRT-PCR analysis of the immune gene *clec-60* in wild-type N2, *acc-4(ok2371)*, or *acc-4(ok2371);gcy-13p*::*acc-4*::*gfp* animals grown on empty vector or *aex-5* RNAi. Data are the mean ± SEM from three independent experiments, n ≈ 200 per condition. ***p < 0.001 via the t test.

(F) Survival of wild-type N2, *acc-4(ok2371)*, *acc-4(ok2371);acc-4p*::*acc4*::*gfp*, and *acc-4(ok2371);gcy-13p*::*acc4*::*gfp* animals on *S. aureus* at 25°C. Data are the mean ± SEM from three independent experiments, n = 90 per condition. N2 versus *acc-4(ok2371)*

animals; $p < 0.0001$. *acc-4(ok2371)* versus *acc-4(ok2371);gcy-13p*::*acc4*::*gfp* animals; $p < 0.0001$. *acc-4(ok2371)* versus *acc-4(ok2371);gcy-13p*::*acc4*::*gfp* animals; $p < 0.0001$.

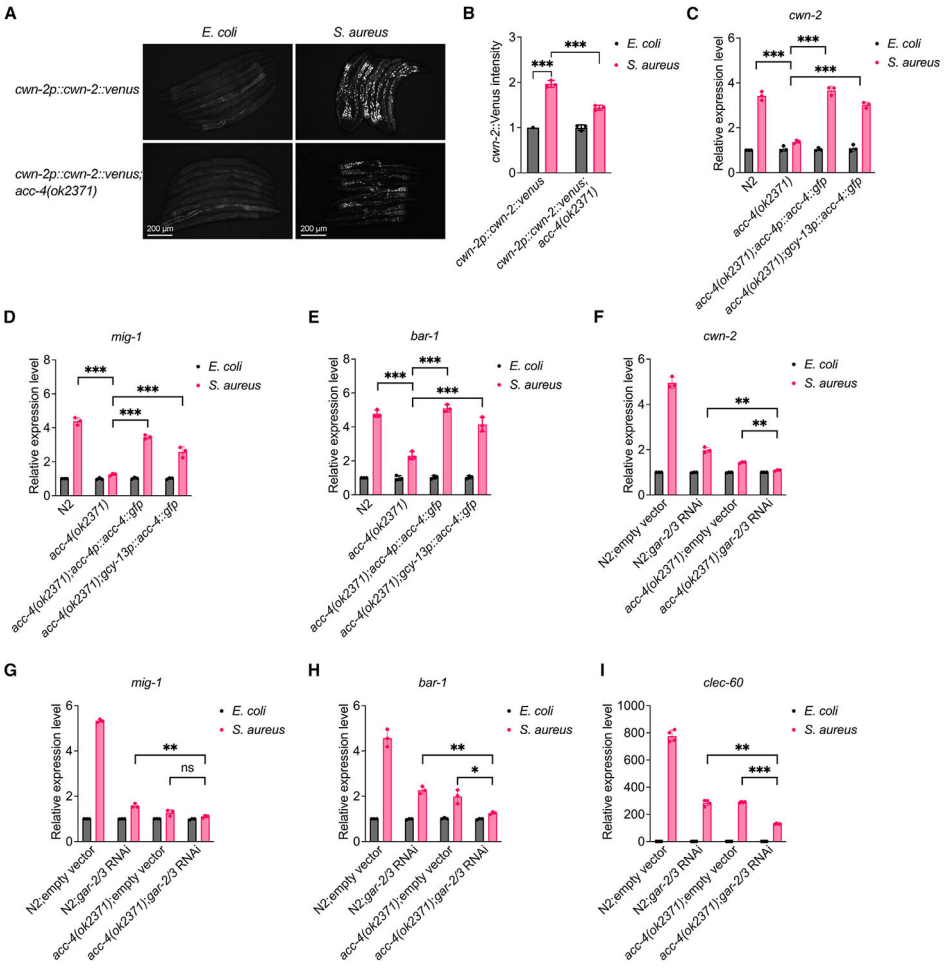

Figure 6. ACC-4 is required for Wnt ligand induction during *S. aureus* infection

(A) Representative epifluorescence micrographs of *cwn-2p*::*cwn-2*::*venus* and *cwn-2p*::*cwn-2*::*venus*;*acc-4(ok2371)* after 16 h of feeding on *E. coli* or *S. aureus*. n = 8; representative of three independent experiments. Fluorescence images were captured using 100-ms exposure. Scale bar, 200 μm.

(B) Quantitative analysis of (A). The height of the columns represents fold changes. Data are the mean ± SEM from three independent experiments, n = 8 per condition. ***p < 0.001 via the t test.

(C–E) qRT-PCR analysis of the Wnt pathway genes *cwn-2* (C), *mig-1* (D), and *bar-1* (E) in wild-type N2, *acc-4(ok2371)*, *acc-4(ok2371)*;*acc-4p*::*acc4*::*gfp*, and *acc-4(ok2371)*;*gcy-13p*::*acc4*::*gfp* after 16 h of feeding on *E. coli* or *S. aureus*. Data are the mean ± SEM from three independent experiments, n ≈ 200 per condition. ***p < 0.001 via the t test.

(F–H) qRT-PCR analysis of the Wnt pathway genes *cwn-2* (F), *mig-1* (G), and *bar-1* (H) in wild-type N2 or *acc-4(ok2371)* animals grown on bacteria carrying empty vector or RNAi against *gar-2* and *gar-3*. Data are the mean ± SEM from three independent experiments, n ≈ 200 per condition. *p < 0.05, **p < 0.01, and ***p < 0.001 via the t test. ns, non-significant.

(I) qRT-PCR analysis of *clec-60* in wild-type N2 or *acc-4(ok2371)* animals grown on bacteria carrying empty vector or RNAi against *gar-2* and *gar-3*. Data are the mean ± SEM

from three independent experiments, n ≈ 200 per condition. **p < 0.01, and ***p < 0.001 via the t test.

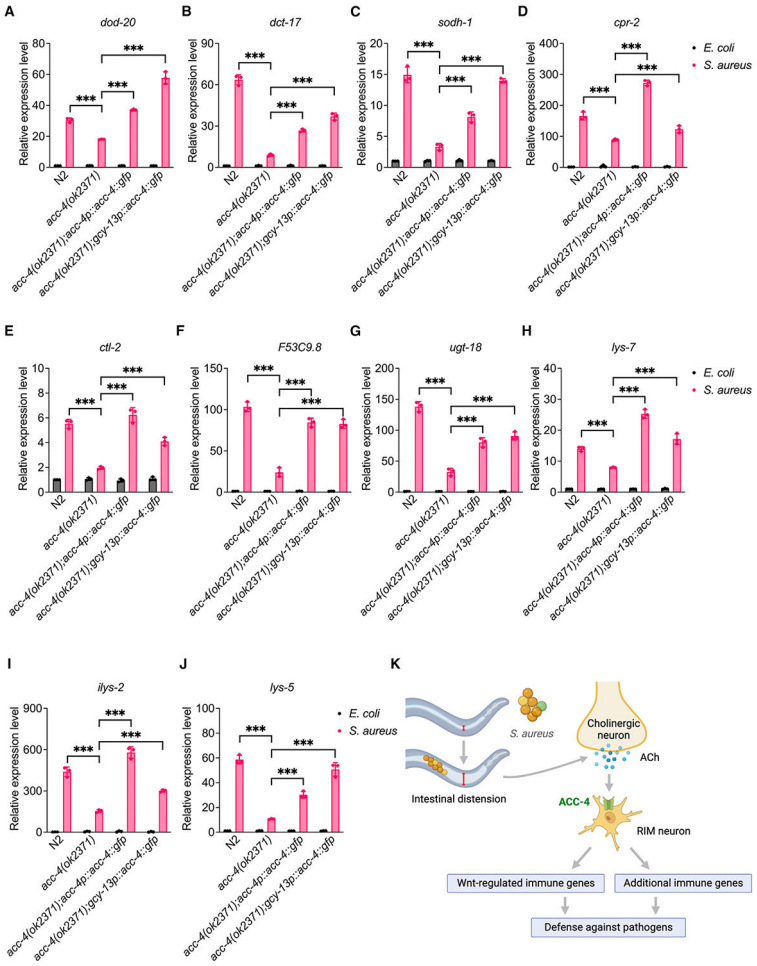

Figure 7. ACC-4 is required for immune activation during intestinal distension caused by *S. aureus* infection

(A–J) qRT-PCR analysis of the immune genes *dod-20* (A), *dct-17* (B), *sodh-1* (C), *cpr-2* (D), *ctl-2* (E), *F53C9.8* (F), *ugt-18* (G), *lys-7* (H), *ilys-2* (I),and *lys-5* (J) in wild-type N2, *acc-4(ok2371)*, *acc-4(ok2371);acc-4p*::*acc4*::*gfp*, and *acc-4(ok2371);gcy-13p*::*acc4*::*gfp* animals after 16 h of feeding on *E. coli* or *S. aureus*. Data are the mean ± SEM from three independent experiments, n ≈ 200 per condition. ***p < 0.001 via the t test.

(K) ACC-4-mediated neuronal signal regulates immune activation during intestinal distension. Infection by *S. aureus* leads to intestinal distension and induces cholinergic neuron release of acetylcholine. The acetylcholine-gated chloride channel ACC-4 functions in RIM to activate Wnt signaling and a broad innate immune response.

KEY RESOURCES TABLE

REAGENT or RESOURCE	SOURCE	IDENTIFIER
Bacterial and virus strains		
Escherichia coli OP50	*Caenorhabditis* Genetics Center	Wormbase ID: OP50
Ahringer RNAi Libraries in *E. coli* HT115 (DE3)	Source BioScience	N/A
Pseudomonas aeruginosa PA14	Laboratory of Frederick M. Ausubel	PA14
*Staphylococcus aureus*NCTC8325	National Collection of Type Cultures	NCTC8325
Chemicals, peptides, and recombinant proteins		
Ethyl-methanesulfonate (EMS)	Millipore Sigma	Catalog No. M0880
Catalog No. M0880	Anatrace	Catalog No. I1003
Proteinase K	QIAGEN	Catalog No. 19131
*Pst*I Restriction enzyme	Thermo Scientific	Catalog No. ER0612
*BamH*I Restriction enzyme	Thermo Scientific	Catalog No. FD0054
*Sal*I Restriction enzyme	Thermo Scientific	Catalog No. FD0644
T4 DNA Ligase	NEW ENGLAND Biolabs	Catalog No. M0202S
Phusion High -Fidelity PCR Kit	NEW ENGLAND Biolabs	Catalog No. M0531S
Dream Taq Green PCR Master Mix (2X)	Thermo Scientific	Catalog No. K1081
Critical commercial assays		
Gentra Puregene kit	QIAGEN	Catalog No. 158667
RNeasy Plus Universal Kit	QIAGEN	Catalog No. 73404
TURBO DNase	Life Technologies	Catalog No. AM1907
High-Capacity cDNA Reverse Transcription Kit	Applied Biosystems	Catalog No. 4368814
Power SYBR PCR Master Mix	Applied Biosystems	Catalog No. 4367659
Experimental models: Organisms/Strains		
N2 C.elegans wild isolate	*Caenorhabditis* Genetics Center	WormBase ID: N2
agIs26 [clec-60p::gfp + myo-2p::mCherry]	*Caenorhabditis* Genetics Center	JIN810
uIs69 [pCFJ90 (myo-2p::mCherry) + unc-119p::sid-1]	*Caenorhabditis* Genetics Center	Tu3401
acc-4(ok2371)	*Caenorhabditis* Genetics Center	CX12724
tdc-1(n3420)	*Caenorhabditis* Genetics Center	MT10661
gcy-13(gk3189)	*Caenorhabditis* Genetics Center	VC3242
flp-11(tm2706)	*Caenorhabditis* Genetics Center	HBR507
wild type *sid-1* V; *uIs69* V [*pCFJ90 (myo-2p::mCherry) + unc-119p::sid-1*]; *agIs26 [clec-60p::gfp].*	This study	AY163
acc-4(ac110) III; *agIs26 [clec-60p::gfp + myo-2p::mCherry].*	This study	AY164
acc-4(ac110) III; *agIs26 [clec-60p::gfp + myo-2p::mCherry]*; *acc-4p::acc-4::gfp*	This study	AY165
acc-4(ac110) III; *agIs26 [clec-60p::gfp + myo-2p::mCherry*]; *gcy-13p::acc-4::gfp*	This study	AY166
acc-4(ok2371) III; *acc-4p::acc-4::gfp*	This study	AY167
acc-4(ok2371) III; *gcy-13p::acc-4::gfp*	This study	AY168
osEx393 [cwn-2p::cwn-2::Venus]	*Caenorhabditis* Genetics Center	HS2332
osEx393 [cwn-2p::cwn-2::Venus];acc-4(ok2371)	This study	AY169

REAGENT or RESOURCE	SOURCE	IDENTIFIER
Oligonucleotides		
See Table S3 for the primers used in the study	Integrated DNA Technologies	N/A
Recombinant DNA		
acc-4p::*acc-4*::*gfp*	This study	N/A
gcy-13p::*acc-4*::*gfp*	This study	N/A
Software and algorithms		
GraphPad Prism	Graph Pad Software, La Jolla, CA	https://www.graphpad.com/scientificsoftware/prism/
Snapgene	GSL Biotech	https://www.snapgene.com
ImageJ	NIH	https://imagej.nih.gov/ij/
Galaxy	N/A	https://usegalaxy.org
Database for Annotation, Visualization, and Integrated Discovery (DAVID)	N/A	https://david.ncifcrf.gov/